ELSEVIER

Contents lists available at ScienceDirect

CIRP Annals - Manufacturing Technology

journal homepage: https://www.editorialmanager.com/CIRP/default.aspx



Experiment and smooth particle hydrodynamic modeling of single-grain diamond scribing of silicon carbide fiber reinforced silicon carbide (SiC_f/SiC)



Hansen Li^{a,*}, Sebastian Prinz^b, Yao Liu^c, Patrick Mattfeld^b, Albert J. Shih (1)^{a,d}

- ^a Mechanical Engineering, University of Michigan, Ann Arbor, USA
- ^b Laboratory for Machine Tools and Production Engineering (WZL), RWTH Aachen University, Aachen, Germany
- ^c Mechanical Engineering, North University of China, Taiyuan, China
- ^d Power Mechanical Engineering, National Tsing Hua University, Hsinchu, Taiwan

ARTICLE INFO

Article history: Available online 13 June 2023

Keywords:
Material removal
Silicon carbide
Smooth particle hydrodynamics modeling

ABSTRACT

The smoothed particle hydrodynamics (SPH) is applied to model the single-grain diamond scribing of the silicon carbide fiber reinforced silicon carbide (SiC_f/SiC). Experiments of diamond scribing on SiC_f/SiC were performed with three parameters: fiber orientation, depth of cut, and speed of cut. The scribing force and 3D shape diamond tip was measured. The SPH simulation based on JH-2 material model of the SiC_f and SiC matrix as well as the experimental modeling is performed. Comparison of SPH-predicted and experimentally measured force identifies parameters for the JH-2 work-material and SPH modeling of SiC_f/SiC for accurate prediction of diamond scribing force.

© 2023 CIRP. Published by Elsevier Ltd. All rights reserved.

1. Introduction

Silicon carbide fiber reinforced silicon carbide (SiC_f/SiC) is a lightweight high-temperature ceramic matrix composite material. SiC_f/SiC has higher specific strength than titanium and nickel-based superalloys above 1000 °C [1] as well as good high-temperature fracture toughness and creep in critical hot sections of aircraft engine and power generation turbines as well as nuclear reactors. SiC_f/SiC is lighter, about 1/3 wt of traditional nickel-based superalloys. The reduced weight and elevated combustion temperature enable the increase of efficiency and thrust of turbines [2,3].

SiC_f/SiC consists of SiC fiber (7.5–15 μ m in diameter) bundles embedded in the SiC ceramic matrix [4]. The fiber-reinforced microstructure of SiC_f/SiC may overcome the limitation on the toughness of monolithic SiC ceramic. To further improve the toughness of SiC_f/SiC, the fiber-matrix is coated with thin (about 0.2 μ m [5]) pyrolytic carbon (PyC) or boron nitride (BN) as the fiber-matrix interfacial coating [6]. To manufacture a SiC_f/SiC part, the SiC_f is first wove into a preform. Chemical vapor infiltration (CVI) is applied to the coating process of the PyC or BN on SiC_f. CVI then fills the porosity of woven and coated SiC_f preform with SiC as the matrix [1].

Diamond grinding is the finishing process to meet stringent dimensional and geometrical tolerances and surface integrity requirements for SiC_f/SiC parts for turbines or nuclear reactors. New SiC_f/SiC grinding techniques have been invented and studied [7]. A better understanding of the material removal and surface damage mechanisms in diamond grinding of SiC_f/SiC is important. However, SiC_f/SiC is hard, brittle, and prone to

* Corresponding author.

E-mail address: hansenli@umich.edu (H. Li).

damage during grinding. Most SiC_f/SiC parts are critical to the safety and reliability of their applications and require damage-free grinding [8].

The single-grain diamond scribing is the foundation to understand the forces and material removal mechanisms in grinding [9]. In this study, the single-grain diamond scribing of SiC_f/SiC is investigated. Zhang et al. [10] studied the effect of yarn orientation and depth of cut on the material removal mechanism in diamond scratching of 2.5D SiC_f/SiC . Yin et al. [11,12] found that high grinding speed reduced the edge chipping in diamond scratching of SiC_f/SiC . Luna et al. [13] revealed that the contact of diamond with SiC_f/SiC determined the initiation of cracks and the SiC_f orientation influenced the cracks propagation.

A model to predict forces in diamond scribing of SiC_f/SiC has not been conducted and is the goal of this research. There are three key challenges for accurate prediction of SiC_f/SiC scribing forces: 1) the complex 3D geometry of SiC_f and SiC, 2) detailed material properties of SiC_f and SiC matrix, and 3) the selection of a simulation method. The finite element method (FEM) [14] is difficult to accurately simulate the deformation and crack propagation in diamond scribing of SiC_f/SiC due to the excess number of elements required. The molecular dynamics (MD) modeling has the nano-metric spatial resolution [15], but is too fine to model the 10-20 µm diameter SiC_f. The smoothed particle hydrodynamics (SPH), a mesh-free Lagrangian method utilizing a set of discrete particles to model the workpiece, is selected to overcome these barriers in modeling. SPH has been applied to model the diamond scratching of ceramics [16,17] as well as the cutting of Ti-6Al-4 V [18], and grinding of bone [19], SiC [20], and blood clot [21]. This research focuses on experimental and SPH modeling of the diamond scribing of SiC_f/SiC. By comparing experimentally measured and SPH-predicted scribing forces, the SiC and SiC_f material properties and configurations of SPH modeling can be validated.

The experimental setup, worn diamond tip shape, and SiC_f/SiC material for scribing of SiC_f/SiC are first presented. The SPH model is described. Results of experimentally measured and SPH-predicted scribing forces are compared and discussed.

2. Experiment single-grain diamond scribing of SiC_f/SiC

Fig. 1(a) shows the experimental set-up with a wheel embedded with a single-grain diamond for scribing, which is inspired by the study of Prinz et al. [22]. The SiC_f/SiC workpiece was mounted on a piezoelectric force dynamometer (Model 9256C1, Kistler) to measure the scribing force with sampling rate of 1 MHz. The force normal to the workpiece surface, denoted as \mathbf{F}_n in Fig. 1(b), is measured. The magnitude of tangential force along the diamond velocity direction is small (about 10% of F_n) with significant fluctuation. Only the F_n is measured in this study.

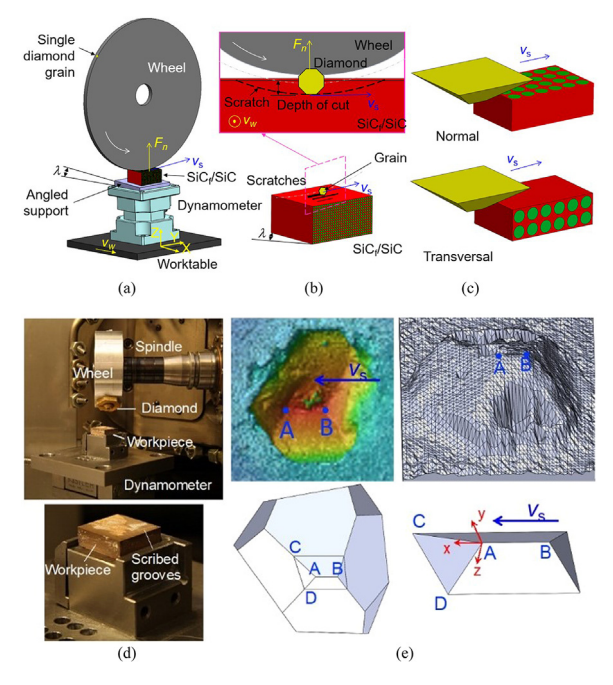


Fig. 1. (a) Configuration of the inclination angle λ for diamond scribing, (b) grooves created in scribing, (c) fiber orientation in normal and tangential orientation, (d) experimental setup, and (e) laser confocal microscope measured diamond shape for 20 m/s v_s , the STL and CAD models of diamond grain, and diamond cutting edges AC and AD.

The experiment plan is to scratch grooves by the diamond (Fig. 1 (b)). It was programmed to scribe the flat polished workpiece surface with several equally spaced scratches of varying depth of cut d_c in a test with the table moving at a speed of v_w . In this study, the d_c was linearly increased and corresponded to the inclination angle λ of the flat SiC_f/SiC surface. This surface was positioned with the SiC_f in normal and tangential orientations (Fig. 1(c)), relative to the diamond velocity vector v_s during scribing. In total, 45 valid grooves were scratched and measured.

The diamond scribing experiment was carried out on a computer numerical control tool grinding machine (Model S22P-turbo, ISOG GmbH) with the diamond, wheel, and workpiece shown in Fig. 1(d). The synthetic 60/70 ANSI mesh MBG 640 cubo-octahedral diamond (Hyperion, Worthington OH USA) was used for scribing. The laser scanning confocal microscope (Model VK-X150 by Keyence) was utilized to measure the shape and identify cutting edges of the diamond. The laser light may penetrate a small translucent region of the diamond and show as cavities, which do not exist on the diamond grain. Fig. 1(e) shows the scanned image of the diamond for scribing at 40 m/s v_s and the edge AB of the diamond. AB is aligned along the scribing direction (Fig. 1(e)) and parallel to the v_s in Fig. 1(a) in the diamond scribing experiment. An XYZ coordinate system (Fig. 1(e)) is defined with point A as the origin. The X-axis is from points B to A. The Z-axis is perpendicular to the workpiece surface. Points C and D are defined to form two cutting edges AC and AD

as well as the surface ACD on the diamond. For v_s = 20 m/s, the diamond grain has the 76.4 μ m length of AB, [0.318, 0.844, 0.431] for the unit vector along AC, and [0.505, -0.634, 0.583] for the unit vector along AD. For v_s = 40 m/s, the length of AB is 38.2 μ m, the unit vector along AC is [0.680, 0.642, 0.355] and along AD is [0.560, -0.606, 0.564]. The diamond defined by four points A, B, C, and D is utilized in SPH modeling.

The SiC_f/SiC workpiece from BJS Ceramics GmbH (Gersthofen, Germany) has the density of $2.3-2.5~g/cm^3$, 280-340~MPa tensile strength, 0.5-0.7% fracture strain, 190-210~GPa Young's modulus, 450-500~MPa bending strength, 10-15~vol% porosity, and 42-47~vol% SiC_f [23].

The specimen surface needs to be flat and damage-free; otherwise, the scribing force will be affected. Multi-stage diamond slurry polishing as fine as 1 μ m grain size was carried out to prepare the surface. Surface polishing may tear the SiC fiber and result in surface damage. Fig. 2(a) shows the scanning electron microscopy (SEM) micrographs of a cross-section of two layers in the woven SiC_f/SiC workpiece. The "fiber ratio" R_f is defined as the area of SiC_f over an area in the cross-section perpendicular to the SiC_f. For example, the lower of Fig. 2(a) has a fiber ratio of 63.4%. The close-up view of the SiC_f, PyC interface, and pore is shown in Fig. 2(b).

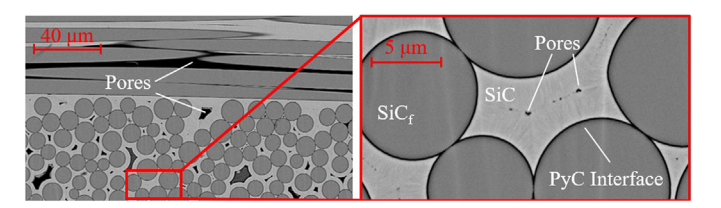


Fig. 2. SEM image of SiC_f/SiC cross-sectional area: (a) across two layers and (b) closed-up view perpendicular to the SiC₆.

3. SPH modeling of diamond scribing of SiC_f/SiC

Fig. 3 illustrates four SPH configurations for the diamond scribing with d_c = 10 and 15 μm and its direction transversal and normal to the SiC_f. The size of the SiC_f/SiC workpiece is 120 μm (width) x 119 μm (length) x 68 μm (depth). This is a small segment within the woven SiC_f/SiC workpiece with uniform SiC_f orientation for scribing. The distance between two SPH particles is 1 μm. The diamond grit trajectory is approximated to be a straight line. The cross-section view of SPH particles at the start of contact between the diamond and workpiece is shown in Fig. 3(a). There are 15 particles across the diameter of a SiC_f. Figs. 3(a) and (b) show the SPH model diamond scribing with transversal fiber orientation and d_c = 10 and 15 μm, respectively. The SPH model of diamond scribing SiC_f in the normal direction with d_c = 10 and 15 μm is shown in Figs. 3(c) and (d), respectively. A total of 1.31 million particles were used in the SPH model.

The shape of diamond defined in Fig. 1(e) is used for scribing. The SiC_f/SiC workpiece in the SPH model is assumed to have a uniform 15 μ m diameter of the SiC_f (the average SiC_f diameter in Fig. 2(a)) and 17 μ m distance between two adjacent axes of two parallel SiC_f (Fig. 3(a)). In this case, the fiber ratio is 61.1%, which is about 5% lower than that measured in SiC_f/SiC in Fig. 2(a) to account for the porosity effect. The boundary condition on the workpiece surfaces is assumed to be fixed except on the top surface and the top half of the front surface where the diamond will first be engaging in contact. The diamond grain (Fig. 1(e)) is assumed to be solid with no deformation. The coefficient of friction between the diamond and SiC_f/SiC is assumed to be 0.35 [20].

The simulation software was LS-DYNA v.13 (ANSYS). The SPH particles have two materials: SiC matrix and SiC_f. The SiC matrix was modelled using the JH-2 constitutive model of SiC [24]. In 1992, to study the ballistic penetration of SiC as the armor material, the JH-1 model was introduced as a constitutive model [25]. In 1994, the JH-2 model was developed adding effects of gradual softening of ceramics and a smoother damage model [24]. In 2003, a new set of JH-2 parameters for SiC was introduced without considering the strain-

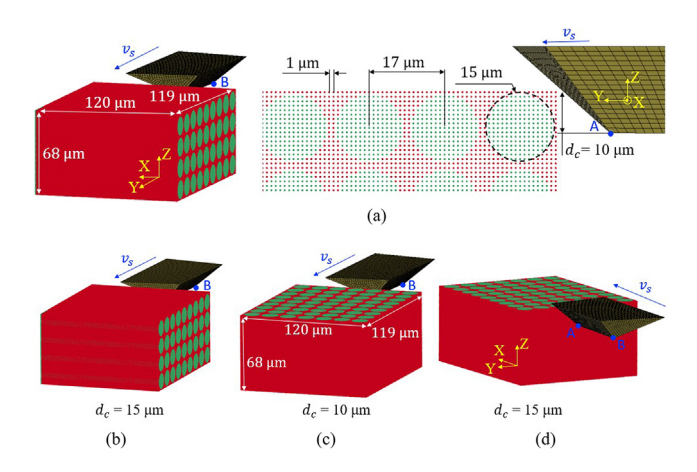


Fig. 3. Four setups for the SPH model of diamond scribing of SiC_f/SiC.

rate effect [26]. Most recently in 2019, the strain-rate effect of SiC was studied for the JH-2 model to improve the dynamic strength prediction. The uniaxial split Hopkinson bar compression tests were conducted on SiC to quantify strain rate parameters in JH-2 model [27]. This JH-2 model is the base of this study. The normalized equivalent stress σ^* , intact strength σ_i^* , and fracture strength σ_f^* are given by [24]:

$$\sigma^* = \sigma_i^* - D(\sigma_i^* - \sigma_f^*); \sigma_i^* = A(P^* + T^*)^N (1 + C \ln \dot{\varepsilon}^*); \sigma_f^*$$

= $B(P^*)^M (1 + C \ln \dot{\varepsilon}^*)$

where the normalized stress σ^* , strain rate ε^* , pressure P^* and maximum tensile hydrostatic pressure T^* are defined as [24]:

$$\sigma^* = \frac{\sigma}{\sigma_{HFI}}; \ \dot{\epsilon}^* = \frac{\dot{\epsilon}}{\dot{\epsilon}_0}; \ P^* = \frac{P}{P_{HFI}}; \ T^* = \frac{T}{P_{HFI}}$$

where σ_{HEL} is the equivalent stress at the Hugoniot elastic limit (HEL). P_{HEL} and L_{HEL} denote the pressure and limit at HEL, respectively. The damage D is an accumulation of increments of plastic strain $\Delta \varepsilon_p$ [24]:

$$D = \sum \left(\Delta \epsilon_p / \epsilon_p^f \right); \ \ \epsilon_p^f = D_1 (P^* + T^*)^{D_2}$$

where ε_p^f is the equivalent plastic strain to fracture under a constant pressure *P*. The hydrostatic pressure *P* can be expressed as [24]:

$$P = K_1 \mu + K_2 \mu^2 + K_3 \mu^3 + \Delta P; \quad \mu = \frac{\rho}{\rho_0} - 1$$

where μ represents the change of density ρ with respect to the initial density ρ_0 . After damage begins to accumulate, the term ΔP becomes a time-dependent variable. After each time interval Δt at time t, the increment of pressure and the expression of elastic energy U are given as [24]:

$$\Delta P_{t+\Delta t} = -K_1 \mu_{t+\Delta t} + \sqrt{\left(K_1 \mu_{t+\Delta t} + \Delta P_t\right)^2 + 2\beta K_1 \Delta U}; \quad U = \sigma^2 / 6G$$

where β represents the fraction of conversion from elastic energy loss ΔU to potential hydrostatic energy gain. More details on the JH-2 model can be found in reference [24].

The 19 parameters for the JH-2 model used in this study are summarized in Table 1. Failure strain FS is set to be 0.2 [27] for both the SiC matrix and SiC_f. This set of parameters is important as the base for future grinding modeling of SiC-based materials.

Table 1Parameters in JH-2 model for SiC matrix and SiC_f [27,28]

| Α | 0.96 | ${\varepsilon_0}^*$ | $1.00 \ s^{-1}$ | L _{HEL} | 11.7 GPa | | SiC | SiC_f |
|---|------|---------------------|-----------------|------------------|----------|------------------|------|---------|
| В | 0.35 | $\sigma_{f,\max}^*$ | 0.132 | P_{HEL} | 7.00 GPa | $\rho (kg/m^3)$ | 3163 | 2370 |
| C | 0.09 | β | 1.00 | K_1 | 220 GPa | G(GPa) | 170 | 56.67 |
| M | 1.00 | D_1 | 0.48 | K_2 | 361 GPa | T(GPa) | 0.75 | 3.00 |
| N | 0.65 | D_2 | 0.48 | K_3 | 0 GPa | | | |

4. Results

Results of diamond scribing experiments and SPH modeling are presented in the following two subsections.

4.1. Experimental results of diamond scribing tests

Fig. 4(a) shows the 12 grooves and the 3D view of grooves measured using the laser scanning confocal microscope (Model VK-X150 by Keyence). A sample cross-sectional view of the varying d_c in grooves is also illustrated in Fig. 4(a). The spacing between grooves is 0.5 mm. The maximum d_c is 25 μ m, which corresponds to an effective inclination angle λ of 0.26°. Two SEM micrographs of surfaces after scribing with the SiC_f transversal and normal to the direction of diamond scribing are shown in Figs. 4(b) and (c), respectively. The pull-out of the SiC_f from the surface is apparent in Fig. 4(b) due to the weak bending strength of SiC_f. On the contrary, the cross-section of the 14 μ m diameter SiC_f in Fig. 4(c) showed the smearing of SiC_f and SiC matrix. This difference in failure mechanism will affect the scribing forces.

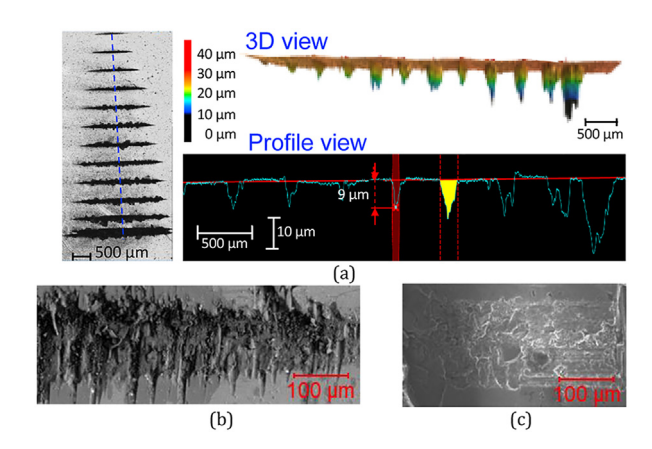


Fig. 4. (a) SEM image of the 12 scribed grooves and the laser confocal scanning and cross-section views. SEM images of the scribed surfaces with $SiC_f(b)$ transversal and (c) normal to the diamond scribing direction.

Measured peak F_n is plotted in Fig. 5 in open circles. F_n increases at a higher of d_c . The regression analysis shows a linearly increasing trend of F_n with respect to d_c . Under both v_s , F_n is larger in the normal (than in transversal) orientation. This can be explained by difference failure mechanisms observed in Figs. 4(b) and (c).

4.2. SPH simulation results of diamond scribing

The peak F_n , sampled at 100 MHz, analyzed using the LSPP (ANSYS) is plotted in Fig. 5 as solid dots. The eight SPH models have a reasonably good prediction of the F_n to distinguish the scribing speed, depth of cut, and fiber orientation effects. The SPH model generally over-predicted the F_n in scribing with the transversal SiC_f orientation. This is likely due to the porosity effect. As illustrated in SEM micrographs in Fig. 2a, pores exist around SiC_f and will reduce its bending strength and the F_n . In the transversal orientation, the porosity effect is more significant. The porosity effect cannot not be distinguished using the fiber ratio parameter, which only considers the overall effect.

Fig. 6 shows the effective plastic strain of SPH mesh when the diamond tool is traveled by 50 μm from the start of contact with 20 m/s speed and 15 μm d_c in transversal and normal fiber orientations. The crack propagation inside the workpiece is revealed by distributions of the effective plastic strain. In both cases, cracks propagate via the interface between fiber and matrix. Fig. 6(a) shows the spread of high plastic strain outside the contact region from the top view, which matches to the fiber pull-out observed in Fig. 4(b) in transversal scribing. In the normal scribing condition (Fig. 6(b)), the high plastic strain occurs below the diamond and it explains the SEM micrograph in Fig. 4(c). This example shows the advantage of SPH modeling to visualize the deformation and material removal mechanism inside the workpiece.

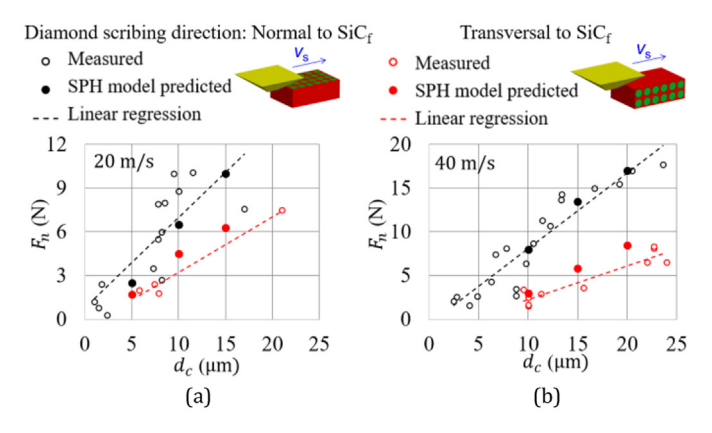


Fig. 5. Comparison of peak F_n from simulations and experiments with v_s of (a) 20 and (b) 40 m/s.

A sensitivity study was conducted to study the distance between two particles, which is a parameter critical for the accuracy of SPH modeling and computational cost. The particle distances of 0.5, 0.67, and 1.0 μ m of the SPH model configuration in Fig. 3(a) were studied at v_s = 40 m/s. Three cases exhibit a similar level of F_n . This study confirms that the 1.0 μ m is adequate for accurate SPH modeling of the diamond scribing of SiC_f/SiC. Another sensitivity study was conducted to study the effect of failure strain (FS), which is unknown for both the SiC matrix and SiC_f. FS = 0.2 is an empirical value used in the previous study under high hydrostatic stress conditions [27]. Eight cases of different combinations of FS for SiC matrix and SiC_f with FS ranging between 0.1 to 0.5 were conducted using the SPH model with transversal SiC_f configuration. No significant change in F_n was observed.

5. Conclusions

This study identified the JH-2 material properties and configuration in SPH modeling to predict the normal force in diamond scribing of SiC_{f}/SiC with a reasonably good agreement. The transversal fiber orientation exhibited a different failure mechanism (Fig. 4) and resulted in lower scribing force (Fig. 5). The scribing depth of cut had a linear trend on F_n . High speed (40 m/s) increased the F_n and this speed effect was significant. This was accurately predicted by selecting the strain-rate effect parameters in the JH-2 model for SiC_f/SiC material.

This study provides a foundation to model the diamond grinding of SiC_f/SiC . The SPH model with evenly distributed SiC_f of equal diameter and proper "fiber ratio" may account for the inherent porosity in the workpiece. The tribological property between SiC_f/SiC and diamond grit still needs more investigation. A single value of the coefficient of friction can predict the F_n but is not adequate to accurately predict the grinding forces. Temperature-dependent material property and thermal effect in the scribing process may need to be considered in the future.

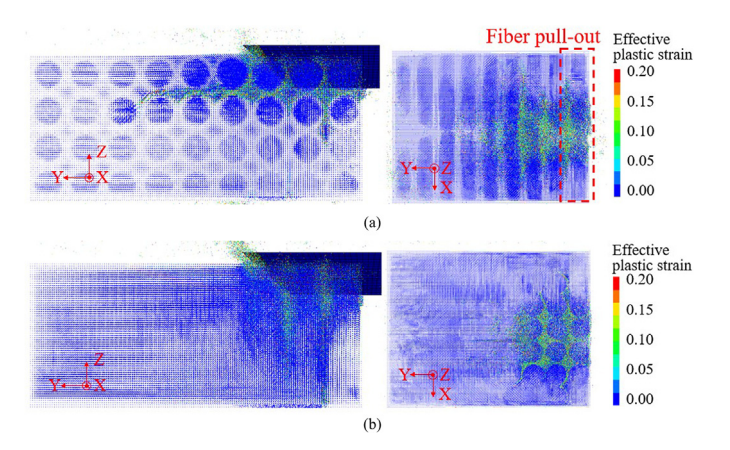


Fig. 6. Effective plastic strain for 20 m/s v_s , 15 μ m d_c , and (a) transversal and (b) normal fiber orientation.

Declaration of Competing Interest

The authors declare that they have no known competing financial interests or personal relationships that could have appeared to influence the work reported in this paper.

Acknowledgments

The authors would like to thank the U.S. National Science Foundation CMMI#1903506 and German Research Foundation BE 2542/7-1 and BE 2542/24-1. Dr. Liu is supported by National Natural Science Foundation of China (NSFC Grant #51905498).

References

- Wang P, et al. (2019) A Review of Third Generation SiC Fibers and SiC_f/SiC Composites. Journal of Materials Science & Technology 35:2743–2750.
- [2] Chamberlain A, et al. (2014) SiC-SiC Ceramic Matric Composites: A Turbine Engine Perspective. ECI Symposium Series, .
- [3] Murthy PLN, et al. (2008) Probabilistic Analysis of a SiC/SiC Ceramic Matrix Composite Turbine Vane. Composites Part B: Engineering 39:694–703.
- [4] Brennan JJ (2000) Interfacial Characterization of a Slurry-cast Melt-infiltrated SiC/ SiC Ceramic-matrix Composite. Acta Materialia 48:4619–4628.
- [5] Li M, et al. (2016) The Effect of the PyC Interphase Coating on the Microwave Heating Sintered SiC/SiC Composites. Journal of Alloys and Compounds 688:974– 981
- [6] Riccardi B, et al. (2004) Issues and Advances in SiCf/SiC Composites Development for Fusion Reactors. Journal of Nuclear Materials 329:56–65.
- [7] Luna GG, et al. (2022) Engineered Grinding Tools Reimplemented by Precise Sharpening: A Case Study on an Ultrahard Ceramic Matrix Composite (CMC). CIRP Annals 71:289–292.
- [8] Bifano TG, et al. (1991) Ductile-Regime Grinding A New Technology for Machining Brittle Materials. *Journal of Engineering for Industry* 113:184–189.
- [9] Liu Y, et al. (2021) Single Diamond Scribing of SiCf/SiC Composite: Force and Material Removal Mechanism Study. *Ceramics International* 47:27702–27709.
- [10] Zhang Z, et al. (2022) Damage Behavior and Removal Mechanism of Different yarn2.5 D SiCf/SiC Composites Under Single-Abrasive Scratch Test. Ceramics International 48:30868–30883.
- [11] Yin J, et al. (2022) Edge Chipping Characteristics in Grinding SiCf/SiC Composite. Ceramics International 48:7126–7135.
- [12] Yin J, et al. (2021) Effects of Grinding Speed on the Material Removal Mechanism in Single Grain Grinding of SiCf/SiC Ceramic Matrix Composite. *Ceramics Interna*tional 47:12795.
- [13] Luna GG, et al. (2020) Influence of Grit Geometry And Fiber Orientation on the Abrasive Material Removal Mechanisms of SiC/SiC Ceramic Matrix Composites (CMCs). International Journal of Machine Tools and Manufacture 157:103580.
- [14] Doman DA, et al. (2009) Finite Element Modeling Approaches in Grinding. International Journal of Machine Tools and Manufacture 49:109–116.
- [15] Lin B, et al. (2003) An Experimental Study on Molecular Dynamics Simulation in Nanometer Grinding. *Journal of Materials Processing Technology* 138:484–488.
- [16] Cao J, et al. (2015) Study on the Material Removal Process in Ultrasonic-assisted Grinding of SiC Ceramics using Smooth Particle Hydrodynamic (SPH) Method. International Journal of Advanced Manufacturing Technology 83:985–994
- International Journal of Advanced Manufacturing Technology 83:985–994.
 [17] Duan N, et al. (2017) SPH and FE Coupled 3D Simulation of Monocrystal SiC Scratching by Single Diamond Grit. International Journal of Refractory Metals and Hard Materials 64:279–293.
- [18] Afrasiabi M, et al. (2021) A Numerical-Experimental Study on Orthogonal Cutting of AISI 1045 Steel and Ti6Al4V Alloy: SPH and FEM Modeling with Newly Identified Friction Coefficients. Metals 11:1683.
- [19] Zheng Y, et al. (2019) Multigrain Smoothed Particle Hydrodynamics and Hertzian Contact Modeling of the Grinding Force in Atherectomy. *Journal of Manufacturing Science and Engineering* 141:041015.
- [20] Liu Y, et al. (2018) Smoothed Particle Hydrodynamics Simulation and Experimental Analysis of SiC Ceramic Grinding Mechanism. *Ceramics International* 44:12194–12203.
- [21] Liu Y, et al. (2019) Cutting of Blood Clots Experiment and Smooth Particle Galerkin Modelling. CIRP Annals 68:97–100.
- [22] Prinz S, et al. (2022) Simulation of material removal behavior during grinding of fiber reinforced non-oxide ceramics (SiC/SiC). *Procedia CIRP*: 2212–8271. (in print).
- [23] Leuchs M, et al. (2002) CVI-Verfahren zur Herstellung faserverstärkter Keramik Herstellung. Keramische Verbundwerkstoffe: 95–121.
 [24] Johnson GR, et al. (1994) An Improved Computational Constitutive Model for Brit-
- [24] Johnson GR, et al. (1994) An Improved Computational Constitutive Model for Brittle Materials. AIP Conference Proceedings, 309.
- [25] Johnson GR, et al. (1992) A Computational Constitutive Model for Brittle Materials Subjected to Large Strains, High Strain Rates and High Pressures. Shock Wave and High-Strain-Rate Phenomena in Materials: 1075–1081.
- [26] Cronin Duane S, et al. (2003) Implementation and Validation of the Johnson-Holmquist Ceramic Material Model in LS-Dyna. 4th European LS-dyna Users Conference, 1.
- [27] Zhang D, et al. (2019) Mechanical Behavior of Silicon Carbide Under Static and Dynamic Compression. Journal of Engineering Materials and Technology 14:11007– 11017.
- [28] Tyranno Fiber UBE Corporation, https://www.ube.com/contents/en/chemical/ continuous_inorganic_fiber/tyranno_fiber.html.